# Supporting Information

# Toward the Next-Generation Nanomedicines: Design of Multifunctional Multiblock Polyurethanes for Effective Cancer Treatment

*Mingming Ding,[†] Nijia Song,[†] Xueling He,[‡] Jiehua Li,[†] Lijuan Zhou,[†] Hong Tan,[†,*] Qiang Fu[†] and Qun Gu[§]*

[†]College of Polymer Science and Engineering, State Key Laboratory of Polymer Materials Engineering, Sichuan University, Chengdu 610065, China, [‡]Laboratory Animal Center of Sichuan University, Chengdu 610041, China, and [§]Ningbo Key Laboratory of Polymer Materials, Ningbo Institute of Material Technology and Engineering, Chinese Academy of Sciences, Ningbo 315201, China

## Supporting Materials and Methods

*Synthesis of Multifunctional Multiblock Polyurethanes (MMPU)*

To obtain MMPUs, a series of functional monomers including L-lysine-derivatized gemini quaternary ammonium salts with two primary amine groups (GQA), L-lysine-γ-aminobutyric acid-γ-aminobutyric acid tripeptide, hydrazone-embedded poly(ε-caprolactone) diol (HPCL, MW 3428) and hydrazone-ended methoxyl-poly(ethylene glycol) (HPEG, MW 1956) were synthesized in our laboratory according to previous reports.[1, 2] GQA was chosen for its excellent cell penetrating activity, which enables it to act as a nonspecific ligand to promote the cell internalization of MMPU nanocarriers.[3] Tripeptide was prepared from L-lysine and γ-

aminobutyric (GABA). Lysine is an essential amino acid in human body,[4, 5] while GABA is a non-protein amino acid widely distributed throughout the biological world including the extracts of a wide variety of animals.[6, 7] Therefore, the use of tripeptide can ensure the biocompatibility of polyurethanes as well as their degradation products. Furthermore, tripeptide contains a carboxyl anion group, which can not only confer a negatively charged carrier surface under physiology environment, but also provide active sites for further functionalization, such as ligand conjugation, imaging element incorporation, *etc*. In addition, the length of side chains can be adjusted by changing the number of GABA incorporated into peptide, through which the spacer of functional moieties attached onto the carrier surfaces can be easily controlled. MMPU was prepared *via* a facile three-step polymerization in *N*,*N*-dimethylacetamide (DMAc) (Figure S1). Briefly, poly(ε-caprolactone) diols (PCL, MW 2000, Dow Chemical) or pH sensitive HPCL macrodiol were copolymerized with L-lysine ethyl ester diisocyanate (LDI) for 1 h at 50-60 °C under a dry nitrogen atmosphere in the presence of stannous octoate catalyst. Subsequently, chain extender 1, 3-propanediol (PDO, Flaka chemika, Switzerland) was added and allowed to react with prepolymers for 1 h at 60 °C. Then tripeptide and GQA were added and the reaction was kept for 1 h at room temperature, followed by another 2 h at 60 °C. Finally, methoxyl-poly(ethylene glycol) (MPEG, MW 1900, Acros Organics) or HPEG were used to terminate the polymers at 60 °C for about 6 h. The obtained polyurethanes were precipitated in a mixture of methanol and diethyl ether for three times.

*Preparation of MMPU Nanocarriers*

To prepare multifunctional multiblock polyurethane nanomicelles, 10 mL of MMPU solution in DMAc was added drop-wise (1 drop every 30 s) to 50 mL of deionized water. The solution was then transferred to a dialysis tube (MWCO 3500) and dialyzed against deionized water for about 3 days to remove the organic solvent at room temperature. The micelle solution was

centrifugalized at 3000 r/min for 10 min and passed through a 0.45 $\mu$m pore-sized syringe filter (Milipore, Carrigtwohill, Co. Cork, Ireland).

Anti-epidermal growth factor receptor (anti-EGFR) monoclonal antibody cetuximab (C225) was chemically conjugated to the nanocarrier surfaces through the carboxyl groups of tripeptide. Briefly, 200 $\mu$L of 0.25 M *N*-ethyl-*N*(3-dimethylaminopropyl) carbodiimide hydrochloride (EDC, J&K Chemical Ltd.) and 200 $\mu$L of 0.25 M *N*-Hydroxysuccinimide (NHS, Alfa Aesar) were added to 10 mL of micelle solution (5 mg/mL) in 4-(2-hydroxyethyl)-1-piperazine-ethanesulfonic acid (HEPES) buffered saline (HBS, pH 7.0). The mixture was incubated for 1 h at room temperature, and then adjusted to pH 7.5 with 1 M NaOH. 0.5 mL of C225 solution (1 mg/mL) was added and the mixture was incubated overnight with gentle stirring. The resultant solution was dialyzed against phosphate buffered saline (PBS, pH 7.4) for 48 h, passed through a 0.45 $\mu$m pore-sized syringe filter and freeze-dried for 24 h.

The success of conjugation was verified *via* an enzyme-linked immunosorbent assay (ELISA). The lyophilized samples were rehydrated in $NaCO_3$ buffer, and added (100 $\mu$L/well) to 96-well plate for incubation overnight at 4 °C. The plate was then washed with PBS containing 0.1% Tween-20 and 0.05% $NaN_3$ (PBS/Tween/azide), followed by a single wash with PBS/azide. After incubation with a blocking buffer containing 2% bovine serum albumin (BSA) in PBS/Tween/azide for 2 h, the plate was washed as before. Afterward, a horseradish peroxidase (HRP)-ragged anti-C225 (secondary antibody) was added to each well. The plate was again incubated at 37 °C for 1 h and washed as before. Coloration was initiated by treating with *o*-phenylenediamine (OPD, Sigma, St. Louis, MO) for 30 min at 37 °C in the dark and stopped with 50 $\mu$L of 2 M $H_2SO4$. The absorbance was measured at 490 nm using a Microplate reader (Model 680, Bio Rad Corp.). The spectrophotometer was calibrated with standard 0.5 to 800 ng/mL C225 solutions. Solutions of unconjugated MMPU micelle were

served as a control. The concentration of C225 in the samples was determined by absorbance reading against the standard curve of serial dilutions of C225, and calculated as the weight of antibody associated with unit weight of lyophilized MMPU micelles.

*Measurements*

Gel permeation chromatography (GPC) was performed on a PL-GPC 220 (Polymer Laboratory Ltd., England) using *N,N*-dimethyl-formamide (DMF)/LiBr as an eluent and polymethyl methacrylate (PMMA) as reference. The sample concentration was 1.0 mg/mL, and the flow rate was 1.0 mL/min.

Size exclusion chromatogram (SEC) was carried out on a Waters system comprised of a Waters 515 HPLC pump, a Waters 2487 UV light detector at 280 nm and an Ultrahydrogel 500 column (7.8 mm x 300 mm). A 10 mM PBS containing 300 mM NaCl and 10 mM $Na_2SO_4$ was used as solvent.

Proton nuclear magnetic resonance ($^1$H NMR) spectra were recorded on a Varian unity Inova-400 spectrometer (400 MHz) in DMSO-$d_6$ or $D_2O$ using tetramethylsilane (TMS) as an internal standard. Carbon-13 nuclear magnetic resonance ($^{13}$C NMR) spectra were obtained on a Bruker AV II-600 MHz spectrometer in DMSO-$d_6$.

Transmission electron microscopy (TEM) was carried out on a Hitachi model H-600-4 transmission electron microscope with an accelerating voltage of 75 KV. A drop of micellar solution stained by 1% (w/v) phosphotungstic acid was placed on a copper grid with Formvar film, and then the liquid was blotted off and air-dried before measurement.

Sizes and zeta potentials of polyurethane nanomicelles were measured with a Zetasizer Nano ZS dynamic light-scattering (DLS) instrument (Malvern, UK) at 25 °C at an angle of 90°.

Fluorescence measurements were carried out using pyrene as a hydrophobic probe. Samples were prepared by adding known amounts of pyrene in acetone into a series of vials. Acetone was evaporated and each vial was added with a predetermined amount of micellar solution. The final concentration of pyrene was $5.0\times10^{-7}$ M. All the solutions were equilibrated upon shaking for 2 h at 40-50 °C and incubated overnight at room temperature. Steady-state fluorescence spectra were recorded on a 970 CRT fluorescence spectrophotometer (Shanghai precision & scientific instrument Co. Ltd., China) with bandwidths of 10.0 nm for excitation and 2.0 nm for emission, respectively. The excitation spectra ($\lambda_{em}$ = 372.0 nm) were collected. The intensity ratio of the peak at 334.3 nm to that at 331.2 nm ($I_{334.3}/I_{331.2}$) from excitation spectra is plotted against the log of the MMPU concentration, and the CMCs are calculated accordingly (Figure S4).

*Fluorescence Microscope*

A431 cells and 3T3 cells were seeded in 96-well plates and incubated in a humidified atmosphere of 5% $CO_2$ at 37 °C for 24 h. The cells were then incubated with hydrophobic fluorescent probe nile red (NR, 98.0%, Sigma)-labeled MMPU nanomicelles at a concentration of 0.1 mg/mL at 37 °C for different times. Afterward, the culture medium was removed, and the cells were washed with PBS three times and observed on a fluorescence microscope (TE2000-U, Japan).

*Computational Simulation*

The architectures of polyurethane micelles and drug-loaded micelles were visually demonstrated by computational simulation using a dissipative particle dynamics (DPD) method, which is a mesoscopic simulation technique developed by Hoogerbrugge and Koelman[8, 9] and a powerful tool to investigate the self-assembly of amphiphilic copolymers.[10] The DPD simulations were performed using Materials Studio 5.0 software (Accelrys) on a DELL PowerEdge SC430 server. The system contained MMPU and water (with or without

PTX) in a cubic box of size 20 × 20 × 20 $r_c^3$ with periodic boundary condition. Simple coarse-grained models of these components are illustrated in Figure S15. MMPU is separated into eleven types of beads (LDI1, LDI2, PCL, PDO, GQA1, GQA2, GQA3, TP1, TP2, TP3 and PEG). Water is represented as an individual particle (W), while the molecular structure of PTX is divided into three types of particles (PTX1, PTX2 and PTX3). The calculated interaction parameters in drug-free and drug-loaded MMPU systems at 298 K are given in Table S3 and S4, respectively. Detailed simulation methods and equations can be found in our previous reports.[3, 11, 12]

**Supporting Tables and Figures**

**Table S1.** Theoretical compositions of multifunctional multiblock polyurethanes.

| Samples[a] | Feed ratios (mol) | | | | | | | |
|---|---|---|---|---|---|---|---|---|
| | LDI | PCL | HPCL | MPEG | HPEG | Chain extender | | |
| | | | | | | GQA | PDO | tripeptide |
| H0 | 2 | 0.6 | 0.2 | 0.4 | 0 | 0.1 | 0.5 | 0.4 |
| H20 | 2 | 0.6 | 0.2 | 0.32 | 0.08 | 0.1 | 0.5 | 0.4 |
| H50 | 2 | 0.6 | 0.2 | 0.2 | 0.2 | 0.1 | 0.5 | 0.4 |
| H80 | 2 | 0.6 | 0.2 | 0.08 | 0.32 | 0.1 | 0.5 | 0.4 |
| H100 | 2 | 0.6 | 0.2 | 0 | 0.4 | 0.1 | 0.5 | 0.4 |
| 0HPCL | 2 | 0.8 | 0 | 0 | 0.4 | 0.1 | 0.5 | 0.4 |
| 0GQA | 2 | 0.6 | 0.2 | 0 | 0.4 | 0 | 0.6 | 0.4 |

[a] Multifunctional multiblock polyurethanes are denoted as H*X*, where *X* is the molar content of HPEG in block agent. 0HPCL and 0GQA represent polyurethanes without HPCL and GQA, respectively.

**Table S2.** Molecular weights and molecular weight distributions of multifunctional multiblock polyurethanes before and after degradation at pH~5 for 24 h.

| Samples[a] | $M_n$ (g/mol)[b] | $M_w$ (g/mol)[b] | $M_w/M_n$[b] |
|---|---|---|---|
| H0 | 29800 | 33300 | 1.12 |
| H0 Deg | 6627 | 7282 | 1.10 |
| H50 | 28200 | 47000 | 1.66 |
| H50 Deg | 6269 | 6767 | 1.10 |
| H100 | 27200 | 43500 | 1.60 |
| H100 Deg | 3232 | 3458 | 1.10 |
| 0HPCL | 12500 | 16400 | 1.32 |
| 0HPCL Deg | 5412 | 5887 | 1.10 |

[a] Deg represents MMPU samples after degradation at pH~5 for 24 h. [b] Determined by GPC.

**Table S3.** Interaction parameters $a_{ij}$ in drug-free MMPU system.

| | W | PEG | LDI1 | LDI2 | PCL | PDO | GQA1 | GQA2 | GQA3 | TP1 | TP2 | TP3 |
|---|---|---|---|---|---|---|---|---|---|---|---|---|
| W | 25.00 | | | | | | | | | | | |
| PEG | 25.97 | 25.00 | | | | | | | | | | |
| LDI1 | 104.40 | 137.38 | 25.00 | | | | | | | | | |
| LDI2 | 84.53 | 118.03 | 25.11 | 25.00 | | | | | | | | |
| PCL | 107.57 | 149.81 | 25.76 | 26.28 | 25.00 | | | | | | | |
| PDO | 104.26 | 153.77 | 26.91 | 27.53 | 25.27 | 25.00 | | | | | | |
| GQA1 | 134.96 | 163.82 | 25.04 | 25.32 | 25.56 | 26.76 | 25.00 | | | | | |
| GQA2 | 26.96 | 25.19 | 138.18 | 119.44 | 152.15 | 157.47 | 163.13 | 25.00 | | | | |
| GQA3 | 158.44 | 201.53 | 28.57 | 29.61 | 25.81 | 25.08 | 28.30 | 202.87 | 25.00 | | | |
| TP1 | 119.02 | 145.48 | 25.12 | 25.00 | 26.62 | 28.30 | 25.36 | 144.76 | 30.63 | 25.00 | | |
| TP2 | 64.88 | 89.08 | 27.72 | 26.53 | 30.66 | 32.65 | 29.12 | 89.51 | 37.55 | 27.15 | 25.00 | |
| TP3 | 45.77 | 85.83 | 325.31 | 274.03 | 331.44 | 323.42 | 402.80 | 99.27 | 450.45 | 365.12 | 220.47 | 25.00 |

**Table S4.** Interaction parameters $a_{ij}$ in PTX-loaded MMPU system.

| | W | PEG | LDI1 | LDI2 | PCL | PDO | GQA1 | GQA2 | GQA3 | TP1 | TP2 | TP3 | PTX1 | PTX2 | PTX3 |
|---|---|---|---|---|---|---|---|---|---|---|---|---|---|---|---|
| W | 25.00 | | | | | | | | | | | | | | |
| PEG | 25.97 | 25.00 | | | | | | | | | | | | | |
| LDI1 | 104.40 | 137.38 | 25.00 | | | | | | | | | | | | |
| LDI2 | 84.53 | 118.03 | 25.11 | 25.00 | | | | | | | | | | | |
| PCL | 107.57 | 149.81 | 25.76 | 26.28 | 25.00 | | | | | | | | | | |
| PDO | 104.26 | 153.77 | 26.91 | 27.53 | 25.27 | 25.00 | | | | | | | | | |
| GQA1 | 134.96 | 163.82 | 25.04 | 25.32 | 25.56 | 26.76 | 25.00 | | | | | | | | |
| GQA2 | 26.96 | 25.19 | 138.18 | 119.44 | 152.15 | 157.47 | 163.13 | 25.00 | | | | | | | |
| GQA3 | 158.44 | 201.53 | 28.57 | 29.61 | 25.81 | 25.08 | 28.30 | 202.87 | 25.00 | | | | | | |
| TP1 | 119.02 | 145.48 | 25.12 | 25.00 | 26.62 | 28.30 | 25.36 | 144.76 | 30.63 | 25.00 | | | | | |
| TP2 | 64.88 | 89.08 | 27.72 | 26.53 | 30.66 | 32.65 | 29.12 | 89.51 | 37.55 | 27.15 | 25.00 | | | | |
| TP3 | 45.77 | 85.83 | 325.31 | 274.03 | 331.44 | 323.42 | 402.80 | 99.27 | 450.45 | 365.12 | 220.47 | 25.00 | | | |
| PTX1 | 218.93 | 238.46 | 26.05 | 27.02 | 25.02 | 25.70 | 25.67 | 234.13 | 26.66 | 27.26 | 35.08 | 605.88 | 25.00 | | |
| PTX2 | 373.47 | 382.27 | 34.46 | 37.29 | 27.92 | 25.72 | 33.44 | 372.80 | 25.21 | 38.51 | 55.99 | 944.57 | 29.57 | 25.00 | |
| PTX3 | 115.99 | 152.57 | 25.30 | 25.72 | 25.12 | 25.79 | 25.15 | 153.70 | 26.75 | 25.88 | 29.74 | 353.04 | 25.11 | 30.20 | 25.00 |

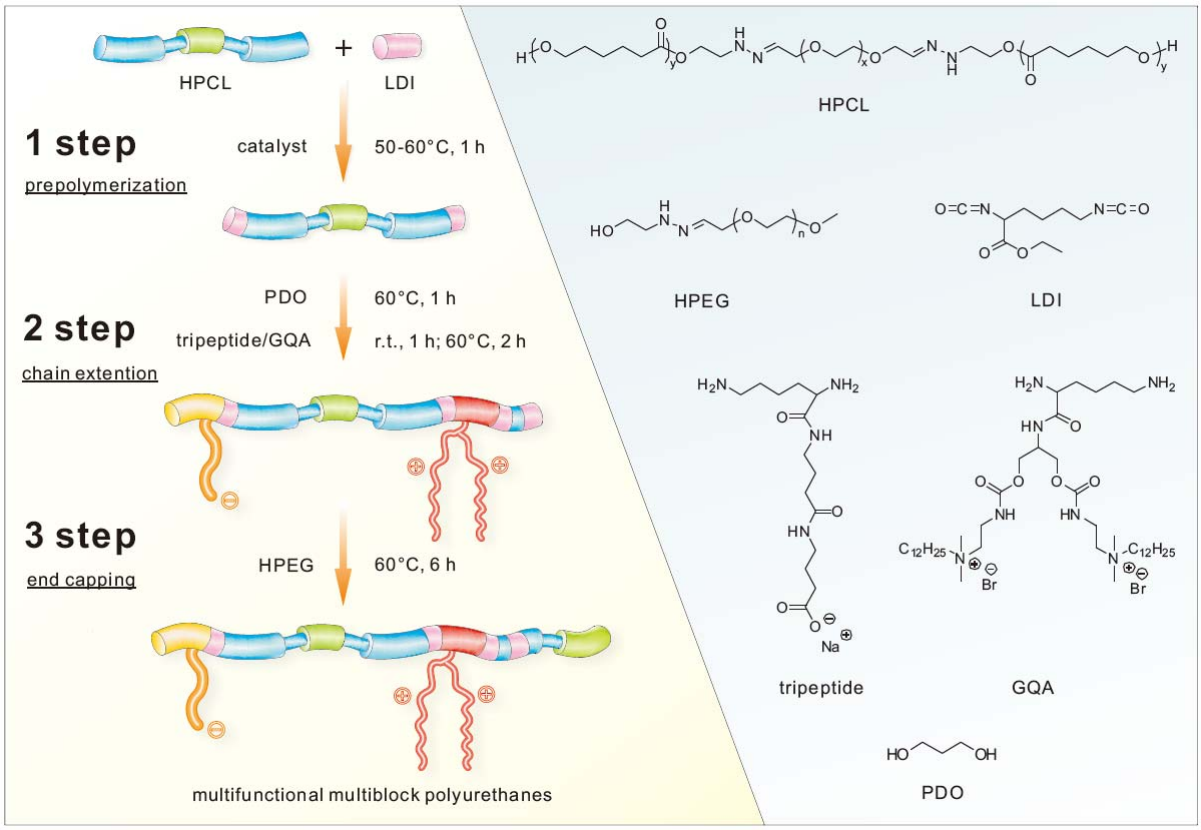


**Figure S1.** Schematic diagrams of three-step polymerization of MMPUs.

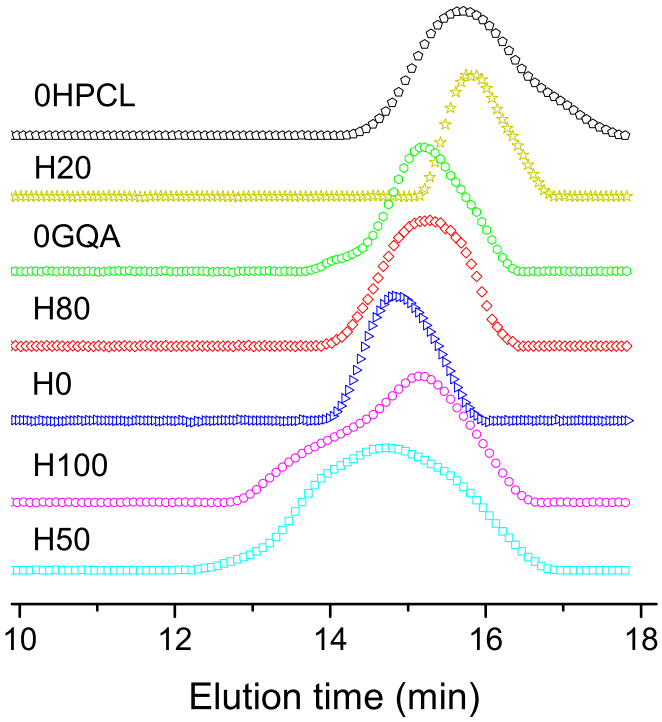


**Figure S2.** GPC diagrams of MMPUs.

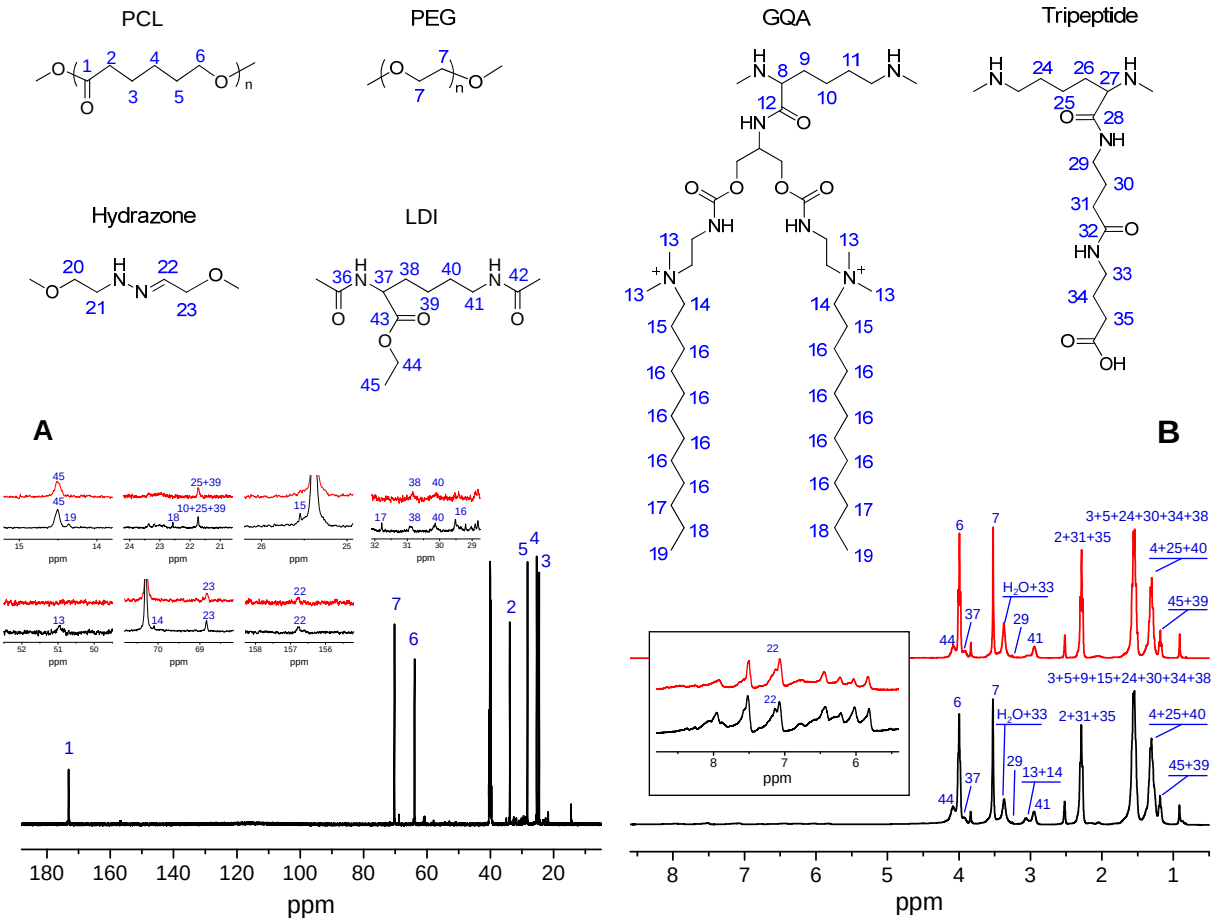


**Figure S3.** 600 MHz $^{13}$C NMR spectra (A) and 400 MHz $^{1}$H NMR spectra (B) of multifunctional multiblock polyurethanes in DMSO-$d_6$. Insets show the partially enlarged spectra. The black lines and red lines indicate H100 and 0GQA, respectively. As seen from $^{1}$H NMR spectra, the peaks at 4.00, 2.29, 1.55 and 1.31 ppm are assigned to the methylene protons of PCL unit. The chemical shifts of methylene and methyl protons in the ethoxyl group of LDI are at 4.09 and 1.19 ppm, respectively. The peak at 3.53 ppm is ascribed to the methylene groups of PEG. The signal at 7.13 ppm is derived from the hydrazone protons. The peak at 3.07 ppm is ascribed to the methyl protons of gemini quaternary ammonium polar groups of GQA. In $^{13}$C NMR spectra, the $^{13}$C resonance signals at 173.1, 64.0, 33.8, 28.3, 25.4 and 24.6 ppm are assigned to the six carbons of PCL unit. The peak at 70.3 ppm is ascribed to PEG segment. The signals at 70.1, 51.0, 29.5, 25.5, 22.6 and 14.4 ppm in the spectrum of H100 can not be found in that of 0GQA, which are derived from the quaternary aminomethyl groups, methylene and terminal methyl group of dodecyl group in GQA, respectively. The signal of hydrazone bond can be found at 156.6 ppm. In addition, the actual composition of MMPU was calculated from the integral area of the $^{1}$H NMR peaks at 1.19 ppm (LDI), 4.00 ppm (PCL), 3.53 ppm (PEG), 3.07 ppm (GQA) and 3.26 ppm (tripeptide). Taken H100 as an example, the LDI/PCL(HPCL)/PEG(HPEG)/GQA/tripeptide block ratios

were determined to be 1.65/0.80/0.15/0.22/0.40, which are close to the trend of corresponding feed compositions (Table S1). These results demonstrate that all the desired functional moieties have been successfully incorporated into MMPUs. It is noteworthy that the PEG incorporated is somewhat less than that designed in MMPU structures, which may be caused by the low reactivity of hydroxy-ended PEG macromer and reduced amount of active isocyanate groups in the end capping process. Therefore, the further optimization of synthesis chemistry and technology is needed to develop MMPU with better-defined and well-controlled architectures. This work is ongoing in our laboratory.

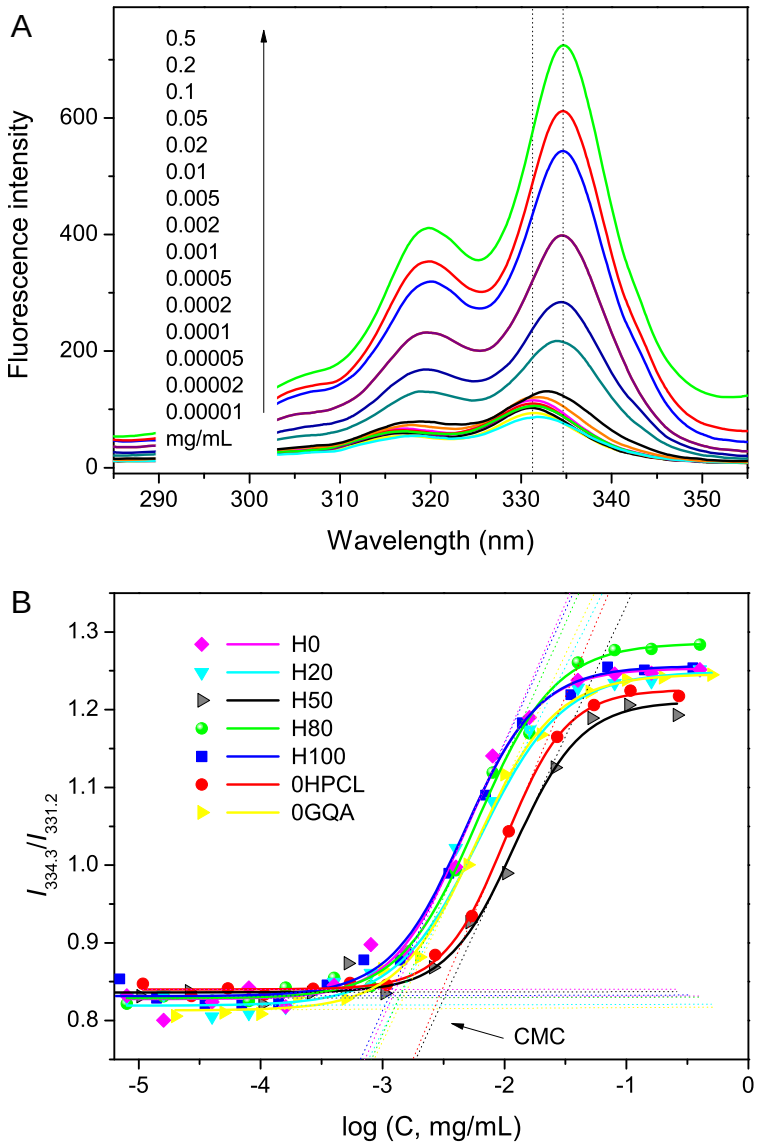


**Figure S4.** (A) Typical fluorescence excitation spectra ($\lambda_{em}$ = 372 nm) of MMPU nanomicelles. As the concentration of MMPU increased, the (0,0) absorption band shifted from 331.2 to 334.3 nm, suggesting that pyrene was located in a more hydrophobic environment. Indeed, this is the evidence for the formation of micellar structure.[13, 14] (B) $I_{334.3}/I_{331.2}$ ratios from pyrene excitation spectra as a function of MMPU concentrations (log *C*) in aqueous solution. The CMCs are obtained from the intersection of the two tangent lines shown by the arrows, and summarized in Table 1.

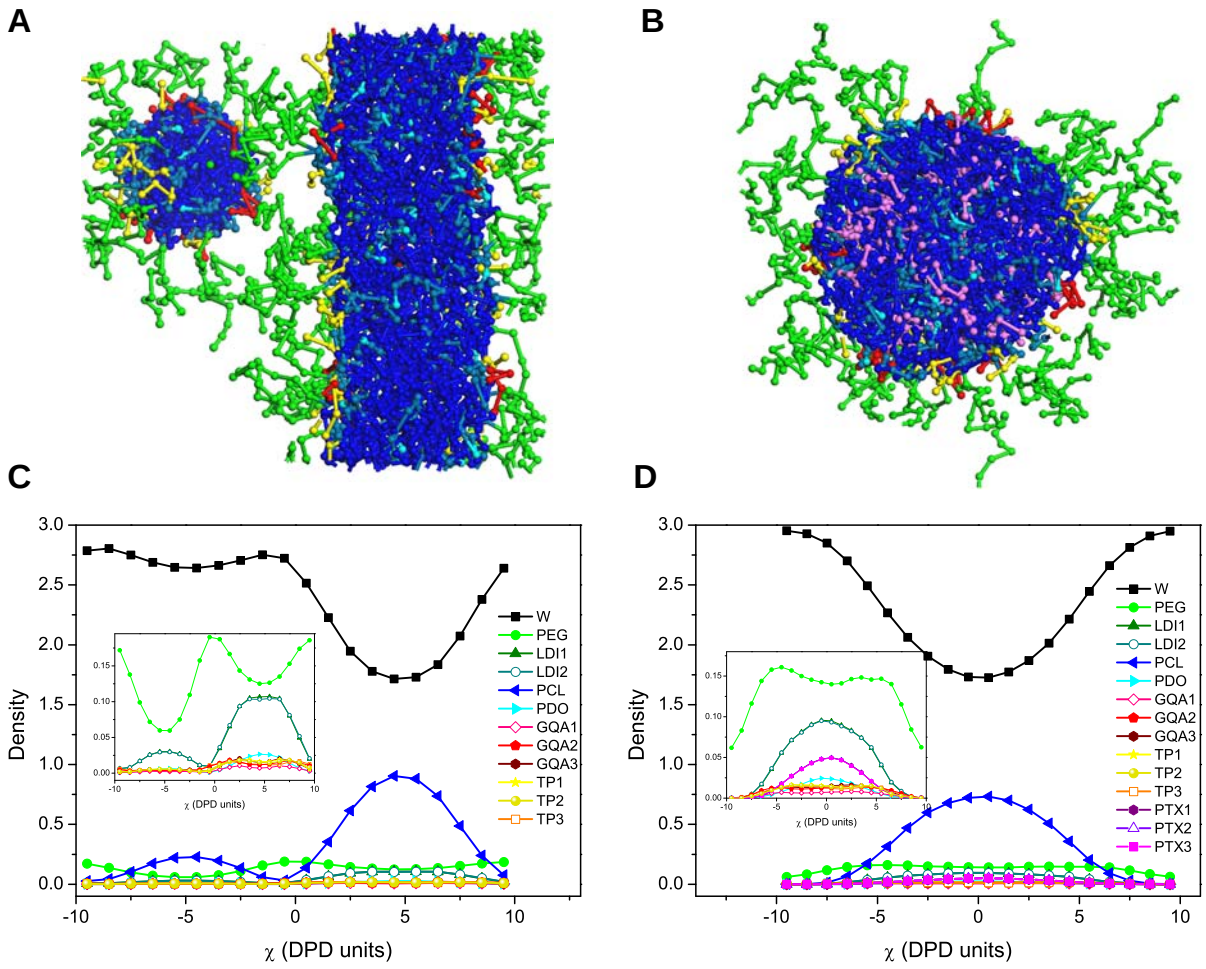


**Figure S5.** Cross-sectional view of micellar structures (A, B) and density profiles (C, D) of MMPU micelles (A, C) and PTX-loaded micelles (B, D) from DPD simulations. Color code: blue, PCL; red, GQA; yellow, tripeptide; green, PEG; magenta, PTX. The insets show enlarged area of density profiles. Evidently, MMPU can self-assemble into a core-shell-corona structure in aqueous solution, where insoluble PCL segment constitutes a hydrophobic core, surrounded by outer shells formed with hydrophilic blocks including GQA, tripeptide and PEG. Since GQA and tripeptide show relatively short chain length and they are connected to hydrophobic PCL blocks through LDI linkages, thus they would form thin layered shells covering the PCL core. In contrast, PEG attached onto the polyurethane chain end have much longer chain length and enough mobility to form an outer corona, which can shield the inner core and thin shells. This result is in good agreement with NMR results (Figure 1 in the manuscript), where the characteristic peaks of PCL, tripeptide and GQA are significantly weakened and even undetected, while that of PEG (3.71 ppm) is clearly enhanced in $D_2O$.

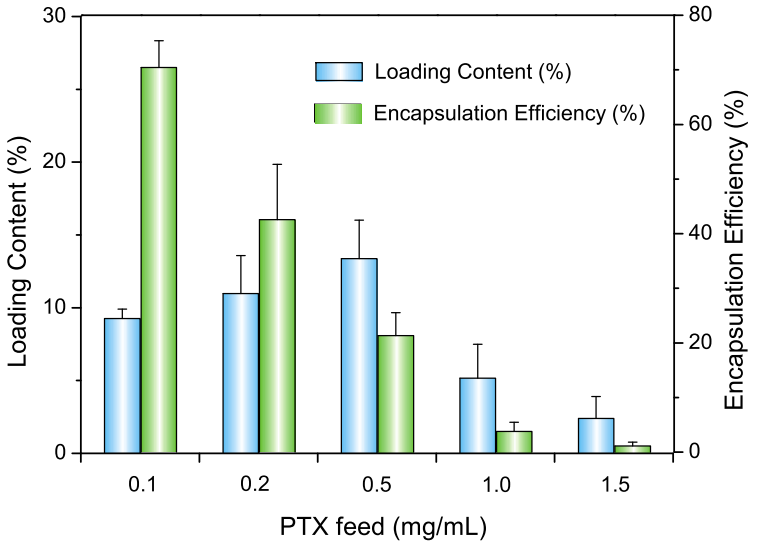


**Figure S6.** Drug loading content and encapsulation efficiency as a function of drug feed ratios for PTX loaded in MMPU (H100) micelles. The drug loading contents increases firstly with the increase of drug feed ratio, and then decreases as the feed concentration of PTX was higher than 0.5 mg/mL, possibly due to the hydrophobic character of PTX.[15, 16]

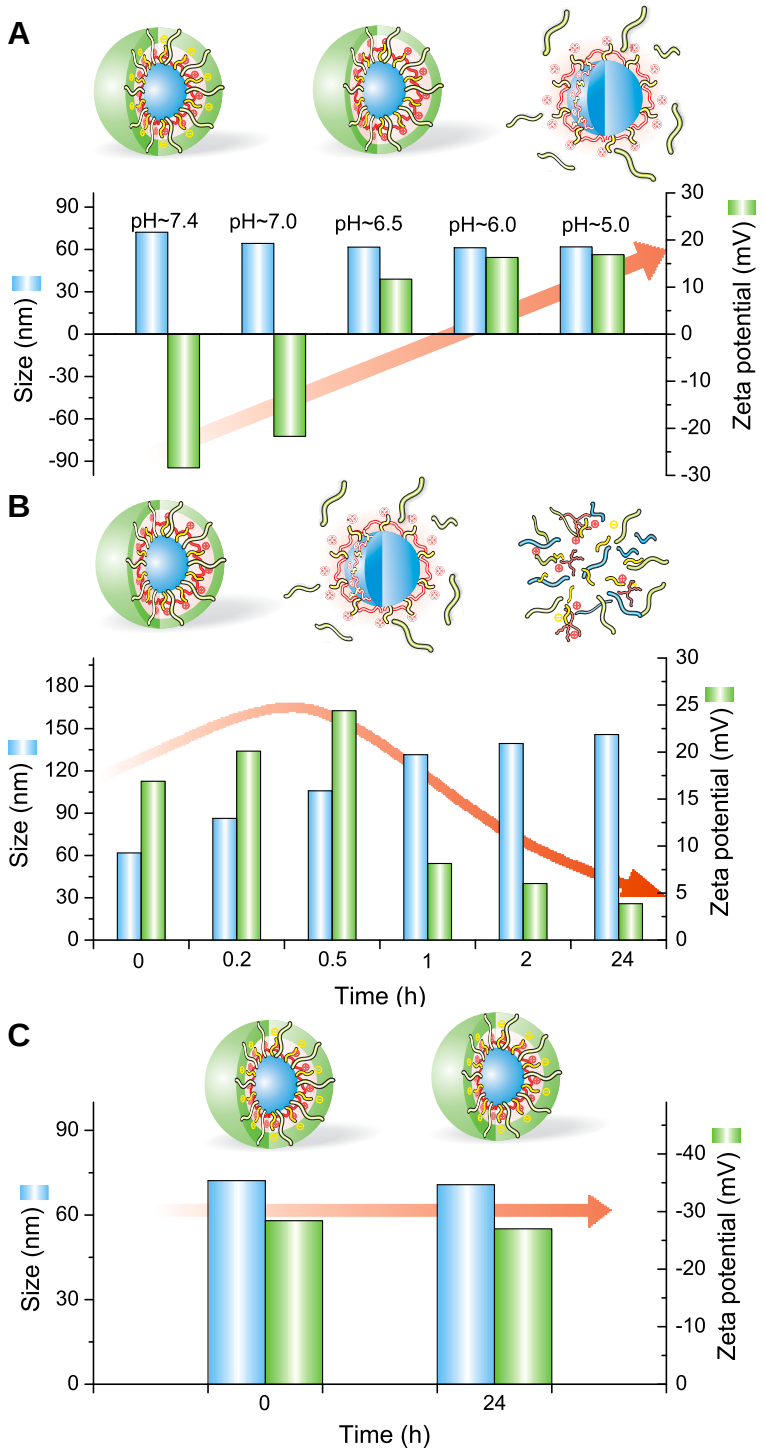


**Figure S7.** The pH-dependant shell-detachment and disintegration behavior of MMPU nanomicelles. (A) MMPU micelle shows negative surface charge under alkalescent and neutral conditions, and becomes positively charged at lower pH values (pH ~6.5-5.0), due to the deionization of carboxyl groups and partial detachment of PEG shell resulting in an exposure of cationic GQA groups. (B) Size and zeta potential of MMPU micelles incubated at pH ~5.0 for different times. The hydrazone linkages attached to the PEG chains at carrier surfaces appear preferentially subjected to acidolysis, rendering a detachment of outer corona

and increase of size and zeta potential before micelle disintegration. With longer incubation at pH ~5.0, the hydrazone bonds embedded in the core-forming PCL block are cleaved and the micelles become disassembled, leading to a decreased zeta potential. (C) Nanomicelle is rather stable under physiological environment (pH ~7.4), with no apparent changes of size and surface charge after 24 h of incubation.

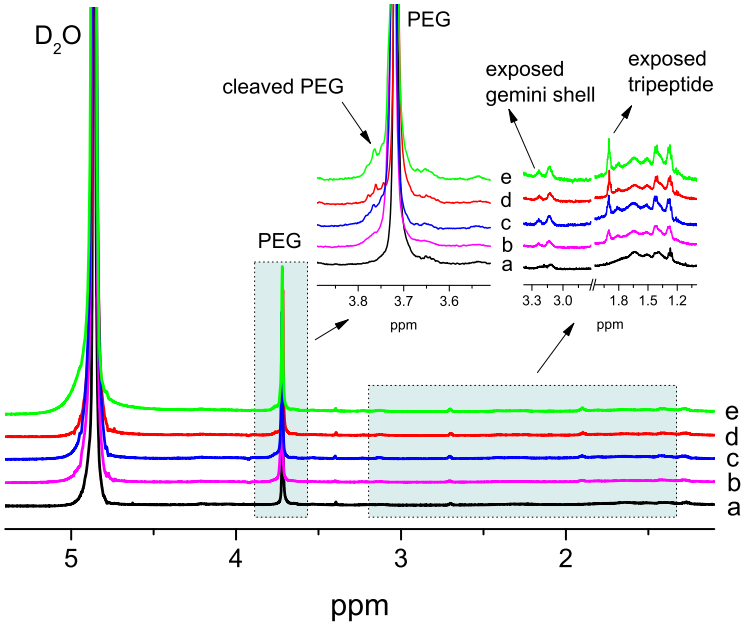


**Figure S8.** 400 MHz $^{1}$H NMR spectra of multifunctional multiblock polyurethane micelles incubated in $D_2O$ (pH ~5) for different times : (a) 0 min, (b) 30 min, (c) 1 h, (d) 4 h and (e) 24 h. With incubation at pH ~5.0, the hydrazone linkages attached to the PEG chains at carrier surfaces were preferentially subjected to acidolysis. Therefore, the PEG shell was cleaved (3.76 ppm), resulting in the partial exposure of GQA shell (3.23 ppm) and tripeptide (1.91 ppm). As a result, the size and surface charges of MMPU nanomicelles changed accordingly (see Figure S6), and the molecular weights of polyurethanes were significantly decreased (see Figure S8).

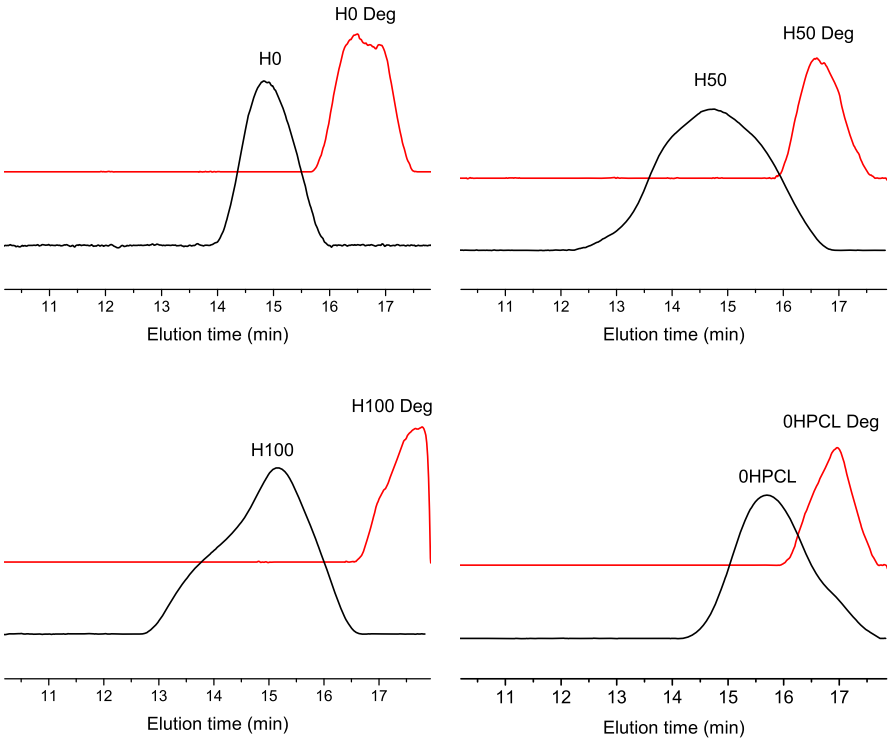


**Figure S9.** GPC diagrams of multifunctional multiblock polyurethanes before and after degradation at pH ~5 for 24 h. Deg represents MMPU sample after degradation at pH~5 for 24 h.

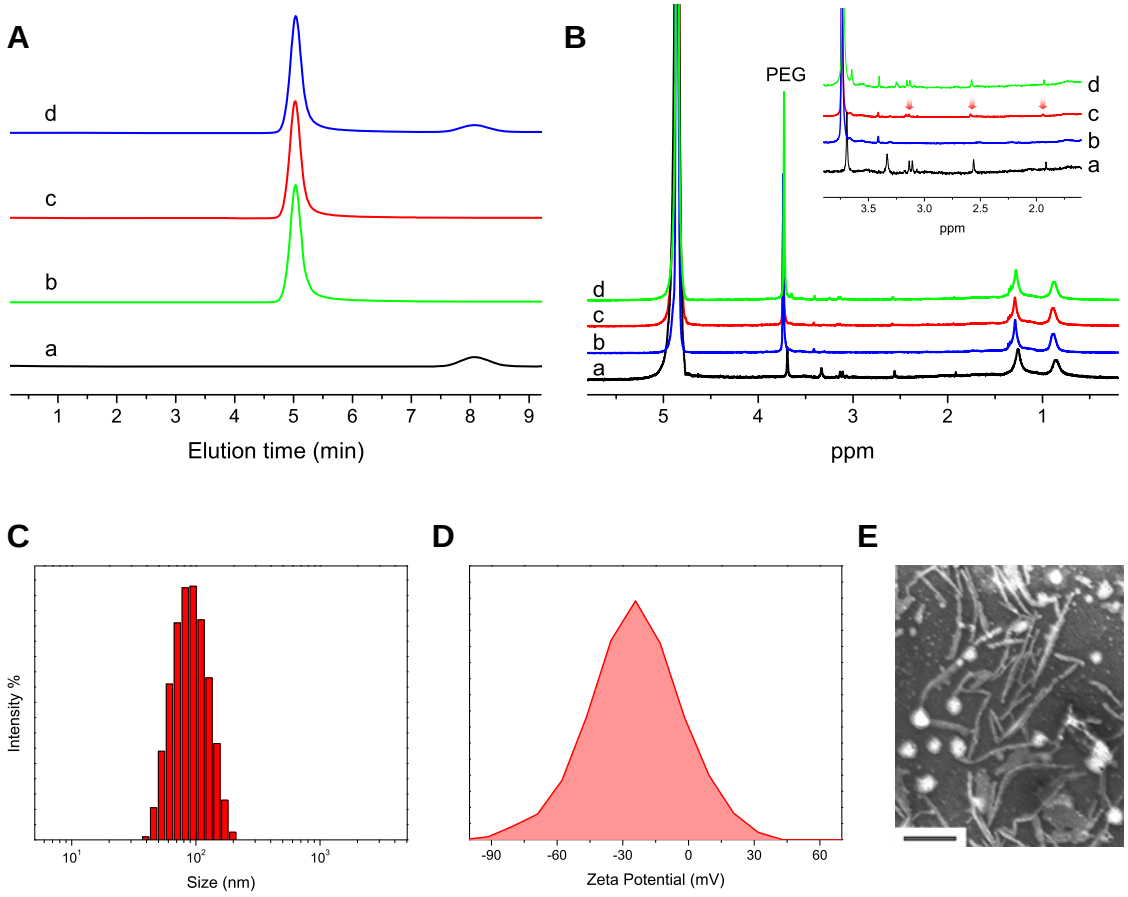


**Figure S10.** (A, B) size-exclusion chromatogram (SEC) traces (A) and 400 MHz $^1$H NMR spectra (B) of C225-conjugated micelles (GHC), unconjugated micelles (GH), mixture of micelle and antibody (GH + C225) as well as C225 solutions in deuterated phosphate buffered saline. C225 was chemically conjugated to the nanocarrier surfaces through the carboxyl groups of tripeptide. The purity of immunomicelles was first characterized with SEC, where only one peak of micelle was observed on the gel chromatogram and no peak of free antibody was found (A).[17-20] In addition, the characteristic signals of C225 observed in the spectra of GHC can not be found in that of GH, suggesting the C225 antibody has been incorporated into the MMPU nanocarriers (B). The success of conjugation and the specific activity of the immunomicelles were also verified *via* an ELISA assay. The yield of reaction is 32% and the antibody content on the micellar surface is approximately 3.2 μg antibody/mg nanoparticle, as determined by ELISA method. (C-E) Size (C), zeta potential (D) and TEM images (E) of C225-conjugated MMPU nanomicelles prepared from H100. Scale bars, 200 nm. After ligand conjugation, the micellar size increases slightly and the distribution of zeta potential is enlarged (C and D). In addition, the immunomicelles display some irregular spherical and fiber-like shapes (E). A possible explanation is that the attachment of C225 macromolecules

may increase the steric repulsion between the corona chains and disturb the force balance among various parameters affecting the free energy of the system, thus resulting in further aggregation of micelles and the formation of cylindrical micellar structure.[21-23] The accurate mechanism remains unclear and further studies are needed to fully understand this interesting phenomenon.

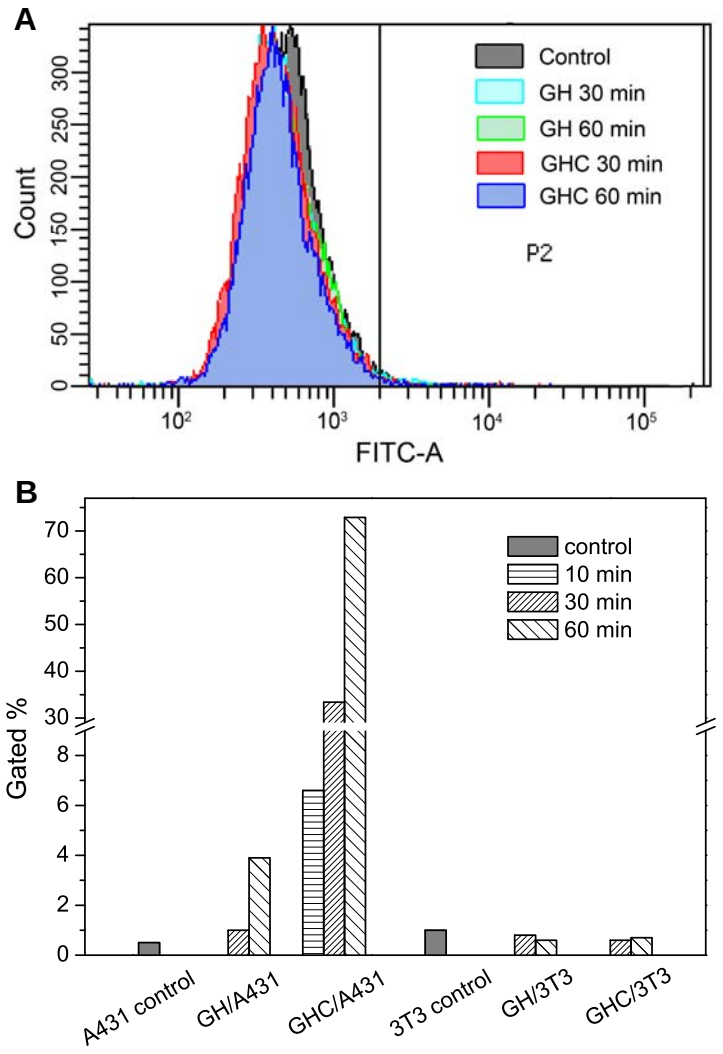


**Figure S11.** (A) Flow cytometry histogram profiles of 3T3 mouse fibroblasts incubated with C225-conjugated MMPU nanocarriers (GHC) and nontargeted nanocarriers (GH) for different times. (B) Internalization efficiency for MMPU nanomicelles with or without C225 after incubation with human A431 squamous carcinoma cells and 3T3 mouse fibroblasts for different times (micelles were labeled with FITC).

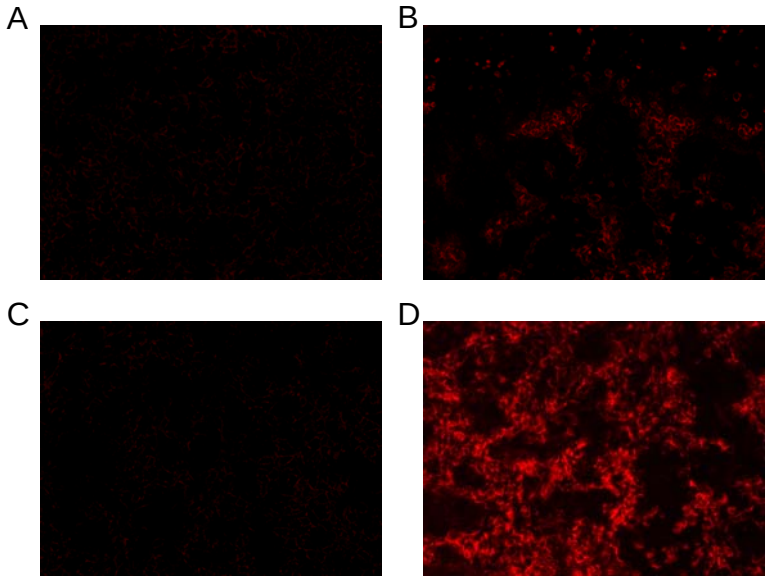


**Figure S12.** Fluorescent microscopy images of 3T3 mouse fibroblasts (A and C) and human A431 squamous carcinoma cells (B and D) incubated with fluorescent-labeled MMPU nanomicelles with or without C225 for 60 min (micelles were labeled with Nile red): (A, B) GH, (C, D) GHC.

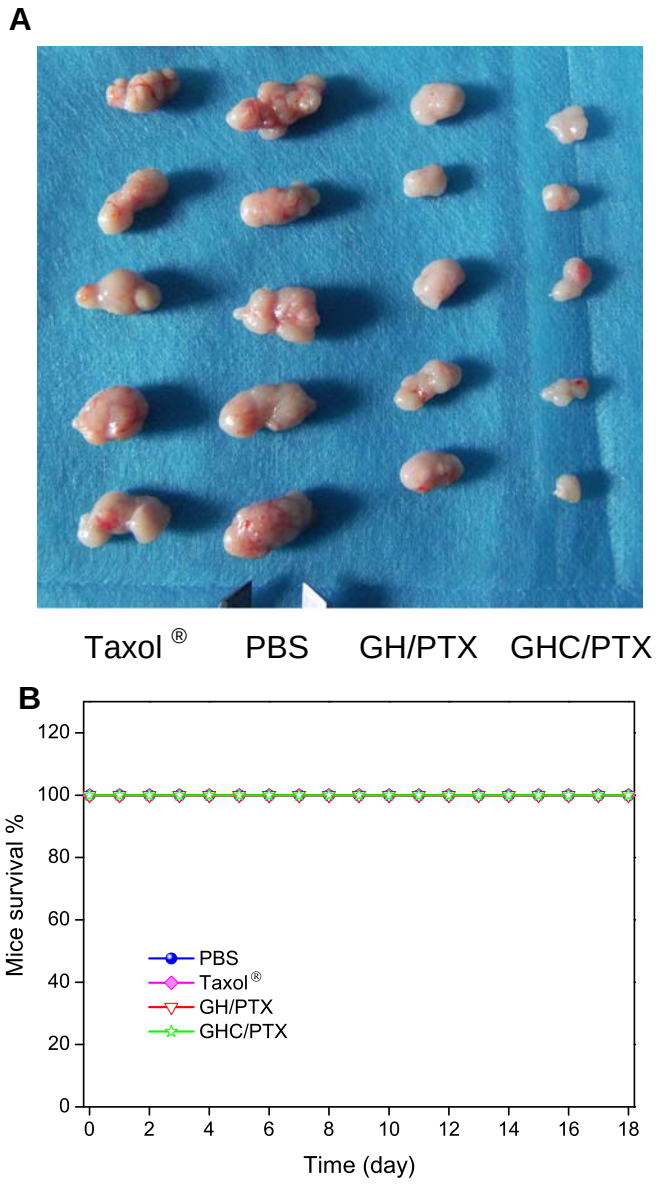


**Figure S13.** (A) Representative tumors separated from animals receiving intravenous injection of Taxol®, PBS, GH/PTX and GHC/PTX formulations. (B) Survival curve of tumor-bearing mice receiving different treatments.

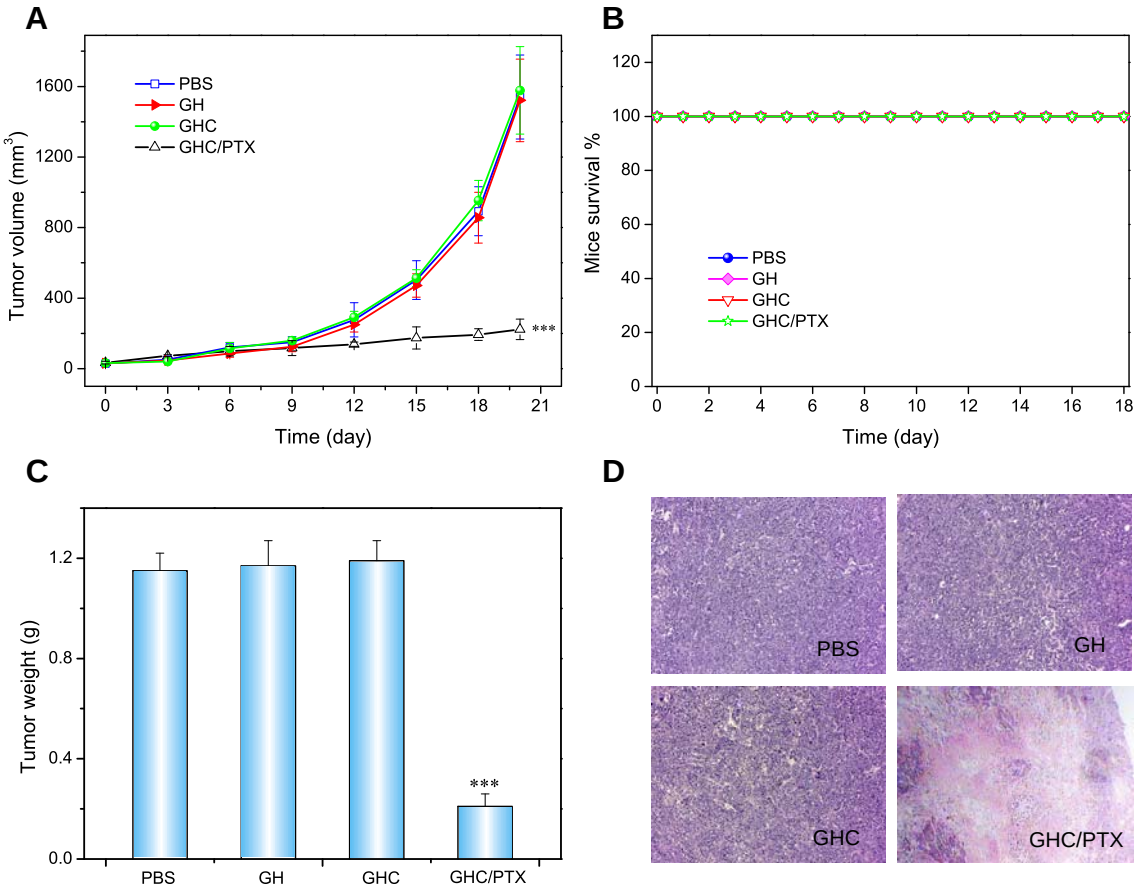


**Figure S14.** (A) Changes of tumor volume after intravenous injection of drug-free GH, GHC and PBS control in A431 tumor-bearing nude mice. (B) Survival curve of tumor-bearing mice receiving different treatments. Mean weights (C) and sections (D) of tumors separated from animals receiving different treatments. Statistical significance: $*P < 0.05$; $**P < 0.01$; $***P < 0.005$. It was found that targeted GHC/PTX formulation displayed significant antitumor effects, while empty micelles (GH and GHC) without drug incorporation did not produce any measurable inhibition effect on tumor growth, revealing that the excellent therapeutic efficacy of GHC/PTX formulation was attributed to targeted delivery of PTX and not to the drug action mediated by C225 itself or other polymer components.

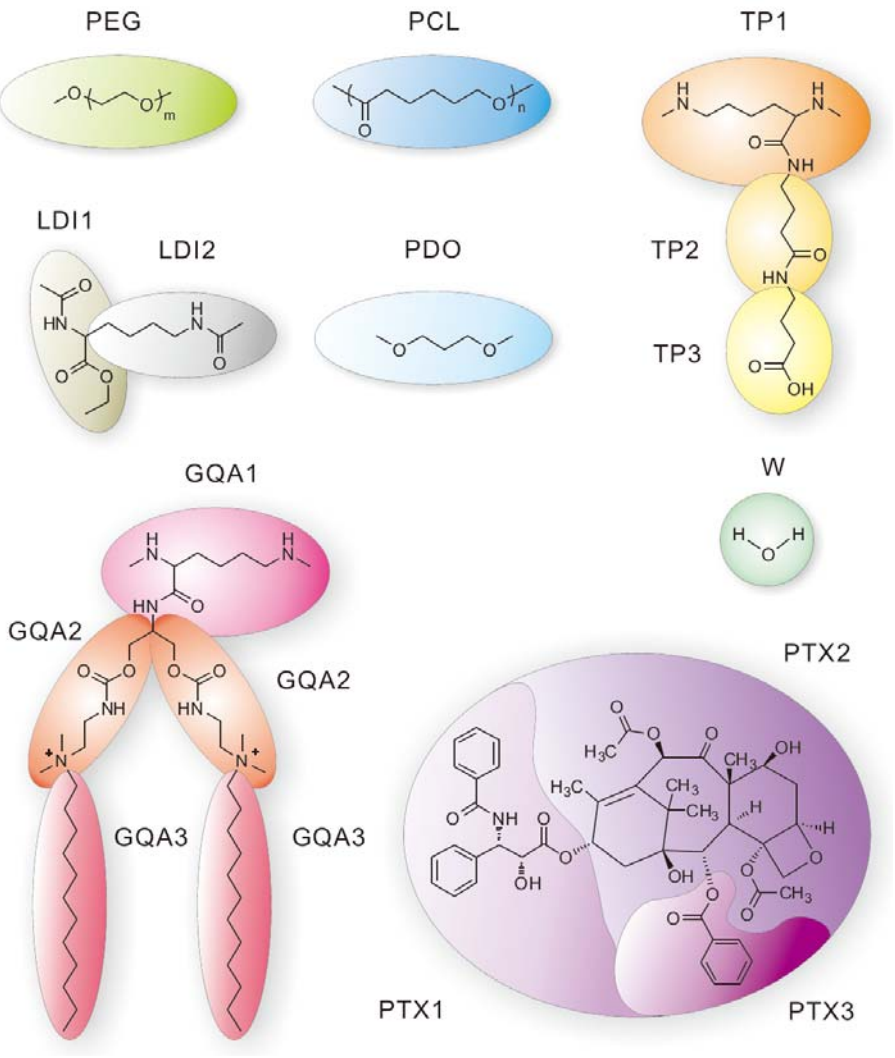


**Figure S15.** Coarse grained models of paclitaxel, water and MMPUs.

**SUPPORTING REFERENCES**


1. Ding, M.; Li, J.; Fu, X.; Zhou, J.; Tan, H.; Gu, Q.; Fu, Q. Synthesis, Degradation, and Cytotoxicity of Multiblock Poly(ε-caprolactone urethane)s Containing Gemini Quaternary Ammonium Cationic Groups. *Biomacromolecules* **2009,** 10, 2857-2865.
2. Zhou, L.; Liang, D.; He, X.; Li, J.; Tan, H.; Li, J.; Fu, Q.; Gu, Q. The Degradation and Biocompatibility of pH-Sensitive Biodegradable Polyurethanes for Intracellular Multifunctional Antitumor Drug Delivery. *Biomaterials* **2012,** 33, 2734–2745.
3. Ding, M.; He, X.; Wang, Z.; Li, J.; Tan, H.; Deng, H.; Fu, Q.; Gu, Q. Cellular Uptake of Polyurethane Nanocarriers Mediated by Gemini Quaternary Ammonium. *Biomaterials* **2011,** 32, 9515-9524.
4. Wu, G. Amino Acids: Metabolism, Functions, and Nutrition. *Amino Acids* **2009,** 37, 1-17.
5. Kasahara, T.; Kato, T. Nutritional Biochemistry: A New Redox-Cofactor Vitamin for Mammals. *Nature* **2003,** 422, 832-832.
6. Kinnersley, A. M.; Turano, F. J. Gamma Aminobutyric Acid (GABA) and Plant Responses to Stress. *Crit Rev Plant Sci* **2000,** 19, 479-509.
7. Zachmann, M.; Tocci, P.; Nyhan, W. L. The Occurrence of γ-Aminobutyric Acid in Human Tissues Other than Brain. *J. Biol. Chem.* **1966,** 241, 1355 -1358.
8. Hoogerbrugge, P. J.; Koelman, J. M. V. A. Simulating Microscopic Hydrodynamic Phenomena with Dissipative Particle Dynamics. *Europhys. Lett.* **1992,** 19, 155.
9. Koelman, J. M. V. A.; Hoogerbrugge, P. J. Dynamic Simulations of Hard-Sphere Suspensions Under Steady Shear. *Europhys. Lett.* **1993,** 21, 363.
10. Guo, X. D.; Tan, J. P. K.; Kim, S. H.; Zhang, L. J.; Zhang, Y.; Hedrick, J. L.; Yang, Y. Y.; Qian, Y. Computational Studies on Self-Assembled Paclitaxel Structures: Templates for Hierarchical Block Copolymer Assemblies and Sustained Drug Release. *Biomaterials* **2009,** 30, 6556-6563.
11. Wang, Z.; Li, J.; Tan, H.; Zhang, X.; Fu, Q. Simulation of Self-Assembly Behaviour of Fluorinated Phospholipid Molecules in Aqueous Solution by Dissipative Particle Dynamics Method. *Mol. Simul.* **2009,** 35, 638 - 647.
12. Li, J.; Chen, Y.; Wang, Z.; Ding, M.; Tan, H.; Fu, Q.; Jiang, X. Synthesis and Self-Assembly of an Amino-Functionalized Hybrid Hydrocarbon/Fluorocarbon Double-Chain Phospholipid. *Langmuir* **2011,** 27, 10859-10866.
13. Wilhelm, M.; Zhao, C.; Wang, Y.; Xu, R.; Winnik, M. A. Poly(styrene-ethylene oxide) Block Copolymer Micelle Formation in Water: A Fluorescence Probe Study. *Macromolecules* **1991,** 24, 1033-1040.
14. Astafieva, I.; Zhong, X. F.; Eisenberg, A. Critical Micellization Phenomena in Block Polyelectrolyte Solutions. *Macromolecules* **1993,** 26, 7339-7352.
15. Park, E. K.; Lee, S. B.; Lee, Y. M. Preparation and Characterization of Methoxy Poly(ethylene glycol)/Poly(ε-caprolactone) Amphiphilic Block Copolymeric Nanospheres for Tumor-Specific Folate-Mediated Targeting of Anticancer Drugs. *Biomaterials* **2005,** 26, 1053-1061.
16. Cheon Lee, S.; Kim, C.; Chan Kwon, I.; Chung, H.; Young Jeong, S. Polymeric Micelles of Poly(2-ethyl-2-oxazoline)-Block-Poly(ε-caprolactone) Copolymer as a Carrier for Paclitaxel. *J. Controlled Release* **2003,** 89, 437-446.
17. Lukyanov, A. N.; Elbayoumi, T. A.; Chakilam, A. R.; Torchilin, V. P. Tumor-targeted liposomes: doxorubicin-loaded long-circulating liposomes modified with anti-cancer antibody. *J. Controlled Release* **2004,** 100, 135-144.
18. Wen, X.; Wu, Q.; Lu, Y.; Fan, Z.; Charnsangavej, C.; Wallace, S.; Chow, D.; Li, C. Poly(ethylene glycol)-Conjugated Anti-EGF Receptor Antibody C225 with Radiometal Chelator Attached to the Termini of Polymer Chains. *Bioconjugate Chem.* **2001,** 12, 545-553.
19. Vega, J.; Ke, S.; Fan, Z.; Wallace, S.; Charsangavej, C.; Li, C. Targeting Doxorubicin to Epidermal Growth Factor Receptors by Site-Specific Conjugation of C225 to Poly(L-Glutamic Acid) Through a Polyethylene Glycol Spacer. *Pharm. Res.* **2003,** 20, 826-832.
20. ElBayoumi, T. A.; Torchilin, V. P. Tumor-Targeted Nanomedicines: Enhanced Antitumor Efficacy *In Vivo* of Doxorubicin-Loaded, Long-Circulating Liposomes Modified with Cancer-Specific Monoclonal Antibody. *Clin. Cancer Res.* **2009,** 15, 1973 -1980.
21. Burke, S. E.; Eisenberg, A. Kinetics and Mechanisms of the Sphere-to-Rod and Rod-to-Sphere Transitions in the Ternary System PS310-b-PAA52/Dioxane/Water. *Langmuir* **2001,** 17, 6705-6714.
22. Yu, H.; Zhu, J.; Jiang, W. Effect of Binary Block-Selective Solvents on Self-Assembly of ABA Triblock Copolymer in Dilute Solution. *J. Polym. Sci., Part B: Polym. Phys.* **2008,** 46, 1536-1545.
23. Zhang, L.; Eisenberg, A. Multiple Morphologies and Characteristics of "Crew-Cut" Micelle-like Aggregates of Polystyrene-b-poly(acrylic acid) Diblock Copolymers in Aqueous Solutions. *J. Am. Chem. Soc.* **1996,** 118, 3168-3181.